# A unified approach for capacity and power based sizing of electric machine and battery in P2 hybrid electric vehicles

# A unified approach for capacity and power based sizing of electric machine and battery in P2 Hybrid Electric Vehicles

Angelo Bonfitto[1], Hadi Rahmeh[1], Nicola Amati[1], Andrea Tonoli[1], Renato Galluzzi[2,*], Sanjarbek Ruzimov[3]

[1]Department of Mechanical and Aerospace Engineering, Politecnico di Torino, Italy

Department of Mechanical and Aerospace Engineering
Politecnico di Torino
Corso Duca degli Abruzzi 24
10129 Turin, Italy
Phone: +39 011 090 6240
Fax: +39 011 090 7963

[2]School of Engineering and Sciences
Tecnologico de Monterrey
Calle del Puente 222
14380 Mexico City, Mexico

[3] Department of Mechanical and Aerospace Engineering
Turin Polytechnic University in Tashkent,
Kichik khalka yuli, 17
Tashkent, Uzbekistan

*Corresponding author

E-mail: renato.galluzzi@tec.mx

## ABSTRACT

Hybrid electric vehicles have proven to be an effective solution for the auto industry to satisfy the increasingly stringent $CO_2$ regulations for the short-medium term. Proper sizing of the different components is required to benefit from the hybrid architecture full potential. This paper proposes a unified method that can be applied in both cases. The method uses the energy flow, storage, and consumption during a cycle to perform the sizing. A 350 V P2 plug-in hybrid and a 48 V P2 mild hybrid are taken as a case study. The sizing is performed by adopting the WLTP cycle and subsequently analyzing the energy profile.

Keywords: *Vehicle electrification, hybrid electric powertrain, battery sizing, electric motor sizing*

## 1. INTRODUCTION

In the last decade, electrified drivetrains have gained a relevant momentum in the automotive market due to the stringent regulations in matter of emissions and fuel consumption [1] [2] [3].

Driven by $CO_2$ legislation, hybrid and electric powertrains have been established as standard solutions in the automotive industry, mainly driven by substantial research efforts in academic and industrial environments. The challenge for carmakers and OEMs is to meet the pollutant limit criteria and, at the same time, satisfy customers' requests in terms of performance, drivability, and cost. In this scenario,

the spread of pure electric vehicles is still largely hindered by limitations in the autonomy range and charging time of the vehicles. HEVs, on the other hand, do not suffer these drawbacks and represent a reliable solution, well accepted by the customers in the current market.

Through recent efforts, car makers have adopted different vehicle architectures. A classification of these layouts can be obtained considering the position of the secondary energy converter or the degree of hybridization based on the electric machine (EM) size. In the first of the three cases, the following schemes are exploited. (**P0**) The alternator mounted on the front-end accessory drive (FEAD) is replaced with a more powerful and efficient EM. The latter assists the ICE at low regimes of driving. Regenerative braking is possible, but its efficiency is low due to the number of dissipative components between the wheels and the EM. Pure electric mode is allowed only for a few kilometers, while the restrictive installation envelope limits the torque and power. (**P1**) The EM is installed on the transmission side of the engine crankshaft. Regeneration from braking is more efficient with respect to P0. The EM can be integrated inside the flywheel, also improving the attenuation of torque oscillations. Stringent requirements about the axial size limit the amount of torque. (**P2**) The EM is located downstream the mechanical clutch. Uncoupling between vehicle and ICE is possible, thus avoiding the drag of the engine inertia and its organic losses during pure electric mode. (**P3**) The EM is installed at the input or output of the secondary transmission shaft. P3 exhibits the same characteristics of P2 and a larger efficiency in regenerative braking. Nevertheless, high values of torque are requested to the EM since no stage of torque amplification is present before the wheels. (**P4**) The EM is installed on the other axle with respect to the one where the ICE is connected. This layout allows for maximum energy recovery from braking, but it complicates the control of the vehicle dynamics. (**P5**) EMs are mounted in the wheels. Torque limitations due to the small axial size of the machine are present [4] [5].

When considering the size of the electric machine as the discriminant of systematization, the following categories are obtained: 1) Micro hybrids. The nominal voltage of the EM is 12 V, only the start

& stop function is allowed; 2) Mild hybrids. The nominal voltage of the EM is typically 48V. Rarely, solutions with 24 V can be found on the market. With this architecture, engine assist and regenerative braking are allowed; 3) Full hybrids. In addition to the previous layouts, capability of battery-only operation is possible; 4) Plug-in hybrids. The main peculiarity is the possibility to connect the battery to the electrical grid and large autonomy range is attainable (around 50-100 km) [6] [7]. The main layout characteristics and functions of HEVs categorized according to the hybridization level systematization are summarized in Table 1.

Table 1. Main characteristics and functions of hybrid architectures [8].

| | | Micro hybrid | Mild hybrid | Full hybrid | Plug-in hybrid |
|---|---|---|---|---|---|
| Properties | Battery voltage [V] | 12 | 24-48 | >200 | >200 |
| | Electric machine power [kW] | 2-5 | 10-20 | 20-50 | 30-120 |
| | Battery chemistry | Lead-acid | Li-ion, NiMH | Li-ion | Li-ion |
| | Battery capacity [kWh] | <1 | <1.5 | <10kWh | <40 kWh |
| | Estimated CO2 emission reduction | <5% | <15% | <20% | <40% |
| Functions | Start & Stop | Y | Y | Y | Y |
| | Boosting | Y | Y | Y | Y |
| | Regeneration from braking (engine off) | N | Y (no P0, P1) | Y | Y |
| | Pure electric mode | N | N | Y | Y |
| | Regeneration from ICE | Y | Y | Y | Y |
| | Cold Engine cranking | N | Y (no P0) | Y | Y |
| | Sailing/Coasting | N | Y (no P0) | Y | Y |
| | Creeping | N | Y (no P0) | Y | Y |

The research effort in vehicle hybridization is currently focused mainly on the energy flow management strategy, battery technology, monitoring techniques for the state of the battery and proper sizing of EM and battery. The latter is of particular importance for all types of hybrids, since insufficient hybridization limits the benefits of the hybrid configuration and wastes possible fuel saving. On the other hand, an excessive hybridization increases the cost without providing any additional benefit or even

reducing the possible fuel saving due to an increase in mass. Several examples of battery and EM sizing can be found in the literature. Usually, to find the best sizing, the fuel consumption and dynamic performance of the vehicle are set as objectives to be optimized and the battery and EM sizes are varied.

Several works regarding the sizing of not off-vehicle chargeable (NOVC) hybrid vehicles have been developed. In his paper, Liao *et al.* [9] studied the best hybridization ratio for two mild and three full hybrid configurations using non-optimal control strategies. In this case study, only an urban driving cycle was considered, since the main fuel saving benefits of hybridization lie in the urban phase. Sundström *et al.* [10] studied the optimal hybridization ratio for mild and full hybrid configurations by using an optimal control strategy – specifically, dynamic programing – to obtain a result that is independent of the control strategy. Later in [11], the results obtained for the mild hybrid were extended, and dynamic programing was used to size a torque-assist hybrid configuration and derive a simple rule-based approach to size this architecture. Lukic *et al* [12] studied the hybridization level for charge sustaining parallel hybrid vehicle. In their analysis, a simple rule-based control was used for energy management. Vehicles with various power capabilities were tested and analyzed to understand the effect of hybridization on the fuel economy and dynamic performance. Galdi *et al.* [13] used a genetic algorithm to size the ICE, EM and battery of a parallel hybrid vehicle. The objective was to minimize the component sizes and harmful emissions. To that end, a cost function was designed by multiplying each of these indices by suitably selected cost factors, while using the vehicle performance as constraint. During simulations, a simple non-optimal control strategy was deployed. Castellazzi *et al.* [14] analyzed the battery sizing for a P4 NOVC hybrid all-wheel drive electric vehicle. In their analysis, a simple on/off control strategy was adopted to split the requested torque between the ICE and EM and four different driving cycles were considered. The sizing was done to obtain the best hybrid performance while limiting the SoC variations, and battery and EM temperatures. The optimal battery size was determined as a function of the electric drive speed.

Similar studies were carried out for off vehicle chargeable (OVC) hybrid vehicles. Madanipour *et al* [15] used a multi-objective algorithm to size the EM, ICE and battery of a plug-in hybrid vehicle using fuzzy logic as an energy management system. The algorithm focused on optimizing the cost, fuel consumption and emission. Hou *et al* [16] studied the optimal battery size for a plug-in hybrid based on the optimal total cost of ownership of a plug-in vehicle in Beijing. The results were compared with the results obtained using the same method for the US market. The study also included a sensitivity analysis based on the battery type and government subsidies. Similarly, Wu *et al* [17] performed the ICE, EM and battery sizing for a plug-in parallel hybrid configuration by optimizing the cost of the vehicle. The cost is optimized by using a parallel chaos optimization algorithm and setting the vehicle performances as constraints. Later, the results' sensitivity to the driving cycle selected for the optimization process and to the performance constraints was evaluated. Hu *et al* [18] performed the battery sizing for a plug-in series hybrid by considering the charging and the on-road energy management strategies. The battery was sized to reduce the $CO_2$ emissions not just for the on-road vehicle, but also taking into account the $CO_2$ emission of the electric grid during recharging.

In this context, most of these studies focus on the sizing of either OVC or NOVC hybrid vehicles only, thus obscuring and undermining the differences or similarities that may exist when sizing two different categories. Furthermore, the effects of the energy flow and distribution between the various powertrain components is often implicit or overlooked. In addition, a majority of the proposed sizing methods are based on optimization algorithms, which can involve multiple iterations and several simulations to achieve their final objective. Also, they may require significant computation time or burden. To address these shortcomings, this study presents a unified approach for battery and EM sizing of both a mild and a plug-in hybrid P2 vehicles. The unified approach is based on the energy distribution and variation during a cycle. Unlike most state-of-the-art solutions, the presented methods require a limited number of simulations and are quick and easy to implement, thereby allowing for a simple preliminary

sizing of the electric components of a hybrid vehicle. In the case of the OVC hybrid, a 350 V P2 plug-in hybrid is considered. Higher priority is given to the full electric operation; thus, the sizing is based on optimizing the electric range. The sizing is done in line with the WLTP regulation and focuses on the battery capacity. Through this paper, this case is referred to as the capacity-based method.

For the NOVC, a P2 mild hybrid at 48 V is considered. The sizing focusses more on assisting the ICE, therefore the sizing is centered on the EM power. In this work, this case is referred to as the power-based method.

The paper is structured as follows. Section 2 presents the proposed methods. Later, section 3 describes the vehicle adopted in this study and its characteristics. Then, Section 4 describes the vehicle modelling and energy management system. Section 5.1 shows the results obtained with the capacity-based sizing. Finally, Section 5.2 shows the results obtained with the power-based approach.

## 2. METHODOLOGY

Two different methods are presented in this study. The first method, the capacity-based approach can be applied on hybrids with OVC capabilities. The method flow is shown in Figure 1. The first step consists in running a single WLTP cycle with the target vehicle with no hybrid functionalities.

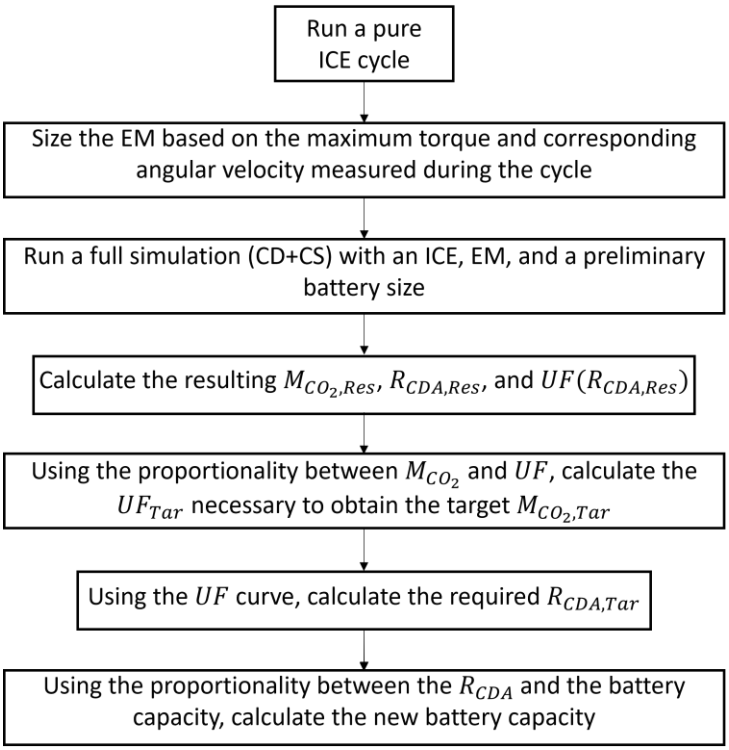


Figure 1. Capacity based approach sizing process

The maximum torque requested by the vehicle and the angular speed of the ICE at which such request occurs are recorded and used as the maximum torque and nominal speed of the EM. Next, using the sized EM, a first tentative battery capacity $E_{Tent}$ is selected, and the vehicle is run in a CD+CS test. The resulting $CO_2$ emissions $M_{CO_2,Res}$, the charge depleting range $R_{CDA,Res}$, and the utility factor $UF_{Res}$ are calculated.

More specifically, according to the WLTP regulation [19]:

- A cycle is considered charge depleting (CD) if on average the battery is discharging and the final SoC of the cycle is lower than the initial SoC.
- A cycle is considered charge sustaining (CS) if the SoC during the cycle respects the following break-off criterion: the difference between the initial and final energy state of the battery should be lower than 4% of the energy required to run a full cycle. Additionally, to avoid implementing a correction procedure to the results, the SoC should be balanced i.e., battery energy should follow an additional criterion: the difference between the initial and final energy state of the battery should be lower than 0.5% of the energy content of the fuel consumed during the cycle. The CS cycle is also referred to as the confirmation cycle, or the n+1 cycle. The last CD cycle is the transition cycle n.

The CO2 emissions average was determined based on the following regulation indication. The average is calculated using equation (1) [19]:

$$M_{CO2,CD+CS} = \sum_{j=1}^{k} \left( UF_j \times M_{CO2,CD,j} \right) + \left( 1 - \sum_{j=1}^{k} UF_j \right) \times M_{CO2,CS} \quad (1)$$

where:

- $M_{CO2,CD,j}$ is the $CO_2$ emission for the phase $j$ in the charge depleting test, g/km
- $M_{CO2,CS}$ is the charge sustaining $CO_2$ emission, g/km
- $j$ is the considered phase (during a single WLTP cycle there are four phases: low, medium, high and extra-high)
- $k$ is the number of phases in the charge depleting test, up to and including the transition cycle
- $UF_j$ is the utility factor of the phase $j$. The capacity of an OVC vehicle to reduce $CO_2$ emissions is highly dependent on the driver's behaviour, i.e., how long is the vehicle driven in electric mode and how frequent are the charging events between trips. To take these factors into

consideration, a utility factor is applied. UFs are ratios based on driving statistics and the ranges achieved in CD mode and CS modes for PHEVs and are used for weighting $CO_2$ emissions and fuel consumptions. The $UF$ varies from 0, meaning no pure electric driving during daily commutes, to 1, meaning full electric driving for the entirety of daily commutes. The $UF$ for phase $j$ is calculated using (2) [19]:

$$UF(d_j) = \phi(d_j) - \sum_{l=1}^{j-1} UF_l \quad (2)$$

where:

- $d_j$ is the distance driven during phase $j$
- $\phi_j$ is determined by interpolating the curve of Figure 2 at the distance $d_j$. The curve is obtained from regulations [20]. It is equal to 0 at 0 km, meaning no weight is given to pure electric driving. Furthermore, it converges to 1 at 800 km, meaning the vehicle is considered driven exclusively in pure electric mode if capable of achieving such range. By the time of the writing of the regulation, data on real world usage of OVC vehicles was rare. As such, the curve is obtained from the statistical study of conventional vehicles databases. The databases include the same database that was used to obtain the WLTP speed profile as well as databases provided by vehicle manufacturers. Although efforts are currently underway to create a UF based on OVC databases [21] [22].

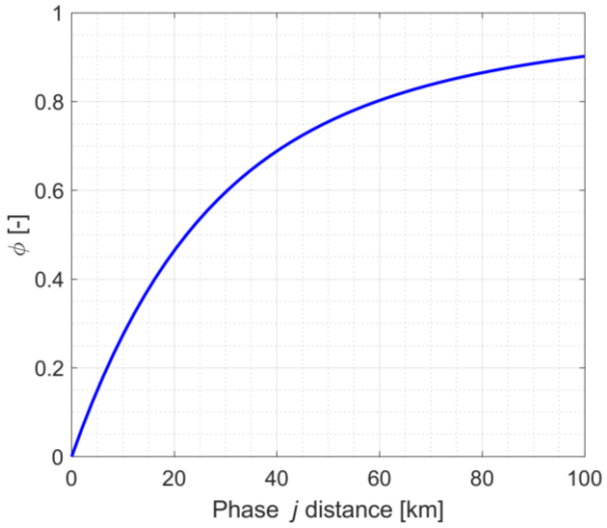


Figure 2. Utility factor estimation

The actual charge depleting range $R_{CDA}$ is determined following the regulation and using (3) [19]:

$$R_{CDA} = \sum_{c=1}^{n-1} d_c + \left( \frac{M_{CO_2,CS} - M_{CO_2,n,cycle}}{M_{CO_2,CS} - M_{CO_2,CD,avg,n-1}} \right) \times d_n \quad (3)$$

where:

- $d_c$ is the distance driven during cycle $c$
- $c$ is the index of the considered cycle
- $M_{CO2,CS}$ is the charge sustaining $CO_2$ emission, g/km
- $M_{CO_2,n,cycle}$ is the $CO_2$ emission of the transition cycle n of the charge depleting test, g/km
- $M_{CO_2,CD,avg,n-1}$ is the arithmetic average CO2 emission of the charge-depleting test from the beginning up to and including the applicable WLTP test cycle $(n-1)$, g/km
- $d_n$ is the distance driven in the transition cycle $n$

Later, the cumulative utility factor $\phi_{Tar}$ corresponding to the desired target $CO_2$ emissions $M_{CO_2,Tar}$ is calculated from the following expression:

$$1 - \phi_{Tar} = \frac{1 - \phi_{Res}}{M_{CO_2,Res}} M_{CO_2,Tar} \tag{4}$$

The matching actual charge depleting range $R_{CDA,Tar}$ can be obtained from the curve of Figure 2. Finally, the required battery size $E_{Tar}$ is determined by considering the linear relation between the battery size and range:

$$E_{Tar} = \frac{R_{CDA,Tar}}{R_{CDA,Res}} E_{Tent} \tag{5}$$

The second method is the power-based approach and is applied on NOVC hybrids. The method is implemented as shown in Figure 3. Again, the first step consists in running the target vehicle without the EM assist.

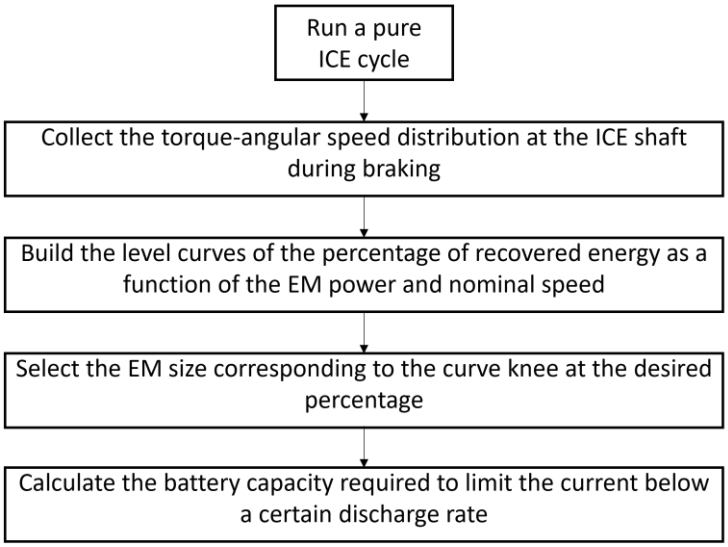


Figure 3. Power based approach sizing process

The braking torque demand at the ICE shaft level and the corresponding angular velocity are collected. From this data, the braking power distribution during the duty cycle can be calculated and integrated to obtain the percentage of recovered energy as a function of the EM maximum power. Once a target energy recovery percentage is selected, the EM which achieves the target recovery with the lowest maximum power and highest nominal speed is chosen.

Finally, once the EM maximum power is set, knowing the battery voltage, the maximum current can be calculated. Considering a limit on the maximum discharge rate, the battery capacity is selected such as to allow the battery to provide the maximum requested current.

## 3. VEHICLE CONFIGURATION

The object of study is a light duty vehicle, whose brand and model are not indicated for confidentiality reasons. However, its characteristics are reported in Table 2. The emissions and fuel consumption results of the conventional ICE-only model were found to match the manufacturer's declared data.

Table 2. Vehicle characteristics.

| Parameter | Value | Unit |
|---|---|---|
| Mass | 3000 | kg |
| Drag coefficient | 0.316 | – |
| Engine characteristics | 2.3L Diesel 101 kW/350Nm | – |
| Battery nominal voltage | 48 | V |
| Transmission | 8-speed automatic | – |
| Transmission ratios (1 to 8) | 4.55, 2.96, 2.07, 1.69, 1.27, 1, 0.85, 0.65 | – |
| Final drive ratio | 3.62 | – |
| Wheel radius | 0.35 | m |
| Rolling resistance | 0.013 | – |
| ICE-only fuel economy | 7.5-7.8 | l/100 km |
| ICE-only $CO_2$ emissions | 198-206 | g/km |

The architecture of the vehicle powertrain is an on axis P2 configuration, schematized in Figure 4.

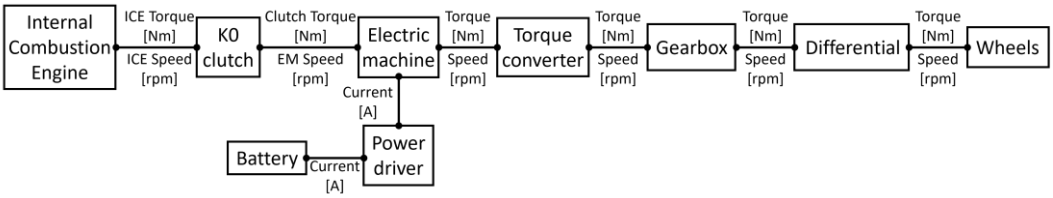


Figure 4. Vehicle powertrain architecture scheme

The ICE is a 2.3 l Diesel engine with a maximum torque of 350 Nm at 2000 rpm, and a maximum power of 101 kW [136 hp]. Figure 5 shows the ICE maximum torque-angular speed characteristic and the brake specific fuel consumption (BSFC) map.

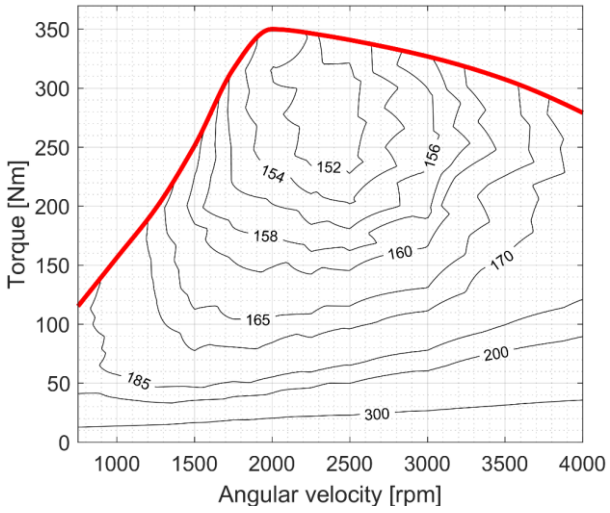


Figure 5. ICE maximum torque characteristic and BSFC map in g/kWh.

A K0 clutch is used to connect the ICE with the rest of the powertrain. When dragged, the ICE suffers inertial load and viscous losses due to the pumped air and lubricating oil, hence decreasing the efficiency of the system. To reduce this effect, while working in full electric mode, the ICE can be disconnected from the rest of the powertrain via the K0 clutch. Thus, the P2 configuration can have several modes of operation that can be set using the K0 clutch: while the clutch is open, the vehicle is capable of

pure electric driving, coasting and regenerative braking. When the clutch is closed, the powertrain is capable of torque assist, power-split or conventional pure ICE driving.

The EM is connected to the automatic gearbox via the torque converter, which prevents the engine from the stalling at low speeds. It is equipped with a locking clutch that remains closed at sufficiently high speeds to prevent viscous losses.

The battery is modelled as a simple ideal voltage source in series with an internal resistance of fixed value. The open circuit voltage varies with the state of charge (SoC), as shown in Figure 6. The SoC to voltage relation is [23]:

$$V = V_0 \left[ \frac{\mathrm{SoC}}{1 - \beta(1 - \mathrm{SoC})} \right] \tag{6}$$

where $V_0$ is the open circuit voltage when the battery is at full capacity, and $\beta$ is a characteristic parameter of the battery. This approximation represents well the open circuit voltage in the SoC range of 10–90%.

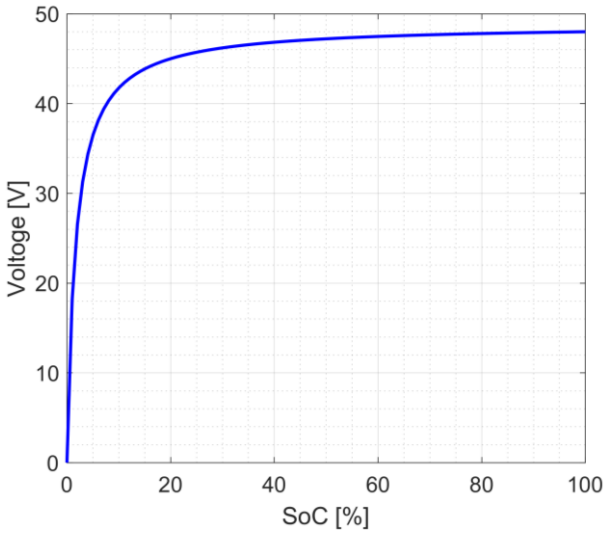


Figure 6. Battery open circuit voltage as a function of SoC.

The current at each time instant is calculated using (7):

$$I(t) = \frac{V(t) - \sqrt{V^2(t) - 4R\frac{T_{em}(t)\omega_{em}(t)}{\eta_{em}^{\mathrm{sign}(T_{em})}}}}{2R} \quad (7)$$

where $\eta_{em}$ is the EM efficiency at the considered EM torque and angular speed, $T_{em}$ and $\omega_{em}$. The battery internal resistance is charge and discharge phases are assumed to be constant over the SOC operation range. Expression (7) is obtained by solving the power balance of the battery considering mechanical power, Joule losses and DC link active power.

# 4. MODELING AND ENERGY FLOW MANAGEMENT

## 4.1. Vehicle model

According to [24], vehicle simulation models can be divided into two main categories: backward (or kinematic) and forward (or dynamic). In the backward model, the vehicle speed is assumed exactly equal to the cycle speed. Thus, using the cycle speed, the acceleration is derived, and the required torque is calculated at every time step. The control strategy then splits the torque demand between ICE, EM and brakes [25].

In the forward model (Figure 7), the vehicle model includes the driver action that typically is represented by a Proportional-Integrative (PI) control law. The PI controller compares the actual vehicle speed with the required cycle speed that is taken as a reference and issues torque commands based on the error between these two signals. The torque command is then fed into the control unit that splits the torque between ICE, EM and brakes. The vehicle speed is then updated based on the produced torque and vehicle dynamics.

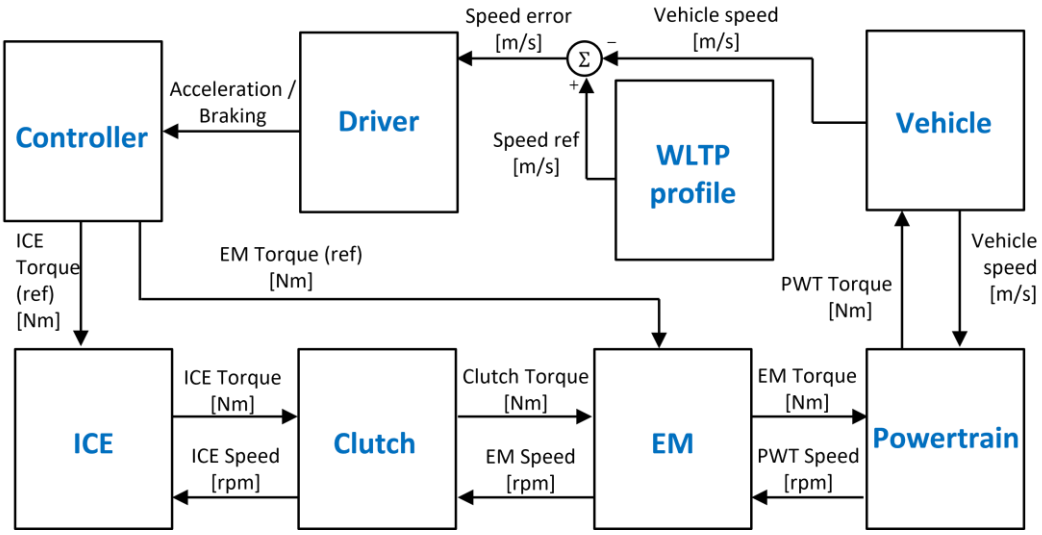


Figure 7. Vehicle forward model.

The backward model is overall simpler to implement and easier to compute, while the forward model is more accurate and realistic by taking into considerations the vehicle dynamics and limits.

In the open loop backward model, the vehicle speed is assumed exactly equal to the cycle speed and therefore, the required torque is calculated directly from the latter. By converse, the closed loop forward model allows for the vehicle dynamics to be taken into consideration and produces a more realistic result.

## 4.2. Control strategy

Hybrid vehicles require a control strategy or energy management system to split the torque command, at every time instant, between the ICE and EM [26]. Control strategies can be split in two main categories: rule-based strategies and model-based strategies. Rule-based strategies, like simple crisp rules or fuzzy logic, do not necessarily require knowledge of the system or its components and are quick and easy to implement, but require considerable tuning to provide near optimal results.

Model-based control strategies require partial or complete knowledge of the system to formulate a cost function. The cost function is then minimized to find the optimal solution. Model-based control strategies can be divided in their turn into two categories: numerical and analytical.

Numerical control strategies, like dynamic programming (DP) or genetic algorithms, can find the absolute best solution to the power distribution between ICE and EM at the lowest fuel consumption. However, numerical control strategies present various disadvantages: the strategy requires prior knowledge of the cycle, it can be only implemented offline, the problem is difficult to formulate, and its solution demands high computational overhead [27] [28].

Analytical control strategies, such as the equivalent consumption minimization strategy (ECMS), are a suboptimal power management strategy capable of yielding results quite close to the optimal solution [29] [30]. ECMS runs in real time and calculates the power share of the ICE and EM at each time instant.

ECMS works by finding, at each instance, the minimum value of the equivalent fuel consumption, expressed in (8):

$$\dot{m}_{f,eqv}(t) = \dot{m}_f(t) + s \cdot \dot{m}_{elec}(t) \tag{8}$$

where $\dot{m}_f$ is the ICE fuel consumption, calculated directly from the ICE BSFC map (such as the one illustrated in Figure 5), $\dot{m}_{elec}$ is the power consumption of the electric motor turned into an associated fuel consumption by following (9):

$$\dot{m}_{elec} = \frac{T_{em}\omega_{em}}{\eta_{em}^{sign(T_{em})}} \frac{1}{Q_{lhv}\eta_{ICE,Max}} \tag{9}$$

$T_{em}$ and $\omega_{em}$ are the EM torque and angular speed, respectively, $\eta_{em}$ is the EM efficiency (which also includes the inverter efficiency) at the considered working point, $Q_{lhv}$ is the fuel lower heating value, and $\eta_{ICE,Max}$ is the ICE maximum efficiency. The latter is assumed equal to $0.4$ in the present study. The battery charge and discharge efficiencies are assumed as unity in the controller.

$\dot{m}_{elec}$ is multiplied by an equivalence factor, which acts as a weighing factor that regulates the contribution of the EM to the total produced torque. A high equivalence factor increases the cost of the consumed battery electricity and thus reduces the EM use, whereas a low equivalence factor promotes the EM use.

As previously explained, the plug-in vehicle will be sized using a capacity-based approach that mainly focuses on the battery sizing, while the mild hybrid vehicle will follow a power-based approach that centres around sizing the EM.

For the capacity-based approach, the $s$ factor is set as a function of the SoC as shown in Figure 8. For a high SoC, the controller promotes a charge depleting operation by setting a very low equivalence factor $S_{low}$. Once the SoC goes below $SoC_{max,1}$, the factor $s$ increases to $S_{mid}$ to promote a charge sustaining operation. The value of $S_{mid}$ is tuned for every simulation to attain the same $SoC$ value at the start of the charge sustaining cycle as the end of the cycle. $S_{high}$ is a safety measure set to protect the battery and avoid draining it below a certain threshold. The two hysteresis triggers ($SoC_{min,1}$ and $SoC_{min,2}$; $SoC_{max,1}$ and $SoC_{max,2}$) prevent fast chattering between two values of $s$ when the SoC is near a threshold.

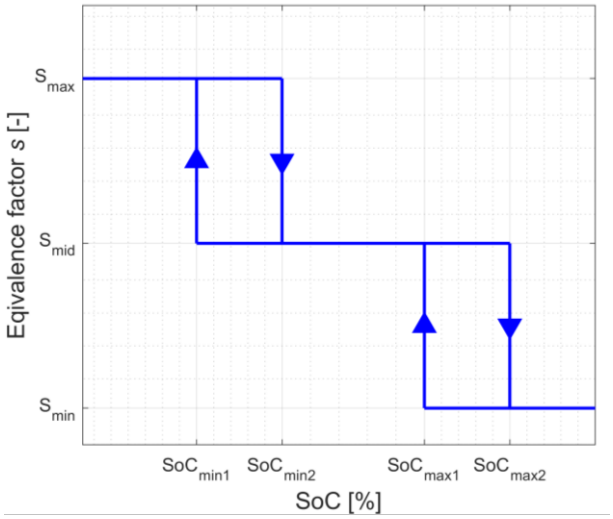


Figure 8. Equivalence factor $s$ as a function of the SoC for the capacity-based approach.

For the power-based approach, the $s$ factor is tuned for every simulation to obtain a charge sustaining cycle, similar to the tuning of $s_{mid}$ in the capacity-based approach.

The ECMS is implemented in the following way: at each time instant, the controller receives the torque request $T_{req}$. The controller discretizes the ICE BSFC and the EM efficiency maps and calculates the equivalent fuel consumption (8) for every combination of $T_{ICE}$ and $T_{em}$ that satisfies the following conditions:

$$\begin{cases} T_{ICE}(t) + T_{em}(t) = T_{req}(t) \\ T_{ICE}(t) \leq T_{ICE\,Max}(\omega_{ICE}) \\ |T_{em}(t)| \leq T_{em\,Max}(\omega_{em}) \\ SoC_{Min} \leq SoC \leq SoC_{Max} \end{cases} \quad (10)$$

$SoC_{Min}$ and $SoC_{Max}$ are two limits imposed on the SoC to avoid damaging the battery. Finally, the controller selects the combination with the lowest equivalent consumption. The control strategy does not take into account the effects of the temperature and the limits it imposes on the maximum available EM torque.

# 5. RESULTS AND DISCUSSION

In the following section, the sizing of the EM and battery for the on axis P2 vehicles is performed. The sizing procedure for the plug-in vehicle follows the capacity-based approach, while the power-based approach is used for the mild hybrid vehicle. In both cases the World-harmonized Light-duty vehicles Test Procedure (WLTP) is adopted. The vehicles are simulated on the WLTP class 3 driving cycle, and their results are subsequently processed following WLTP rules and regulations.

## 5.1. Capacity-based approach

The plug-in P2 on axis vehicle is sized following the capacity-based approach. The EM maximum torque and nominal speed are obtained from the torque request and angular speed locus during a WLTP cycle. Using the obtained EM, several tests are run using different battery capacities. The results show diminishing $CO_2$ saving values for increasing battery capacity levels.

### 5.1.1. Electric machine sizing

The selection of the size of the electric machine is conducted considering the minimum requirements in terms of nominal speed and torque to run the vehicle in pure electric mode in all the possible vehicle conditions.

Based on the results obtained running a WLTP cycle with a pure ICE vehicle, the maximum torque request of 350 Nm is found at an ICE angular velocity of 2500 rpm. Therefore, these torque and speed values are used as the nominal torque and base speed, respectively, for the EM. Figure 9 shows the EM torque characteristic and efficiency map used for the subsequent simulation. Also, the EM parameters are listed in Table 3.

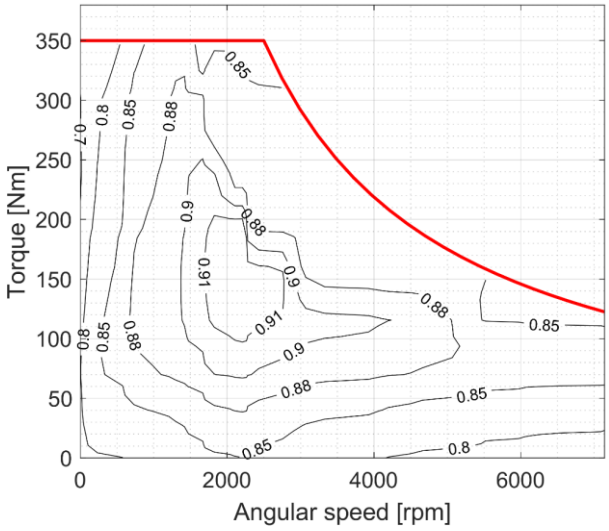


Figure 9. High voltage EM torque characteristic and efficiency map.

Table 3. High voltage EM features.

| Parameter | Value | Unit |
|---|---|---|
| Continuous torque | 175 | Nm |
| Peak torque (<10 s) | 350 | Nm |
| Base speed | 2500 | rpm |
| Max. speed | 7000 | rpm |
| Max. efficiency | 91 | % |
| PM flux linkage | 65.8 | mWb |
| Pole pairs | 9 | – |
| Phase-to-phase resistance | 40 | mΩ |
| Phase-to-phase inductance | 0.23 | mH |
| Saliency ratio | 0.7 | – |

Using the above-mentioned EM in pure electric mode, the vehicle can reach the following performance indices:

- 0 to 50 km/h in 5.4 seconds
- 0 to 120 km/h in 32.4 seconds
- Maximum speed of 150 km/h
- Speed at 6% slope of 103 km/h

- Gradeability at 30 km/h of 32%
- Gradeability at 60 km/h of 12%

Figure 10 shows the working points distribution during a WLTP cycle on the torque characteristic of the EM. The yellow color shows high-density regions, with the number 1 on the scale corresponding to the highest density zone, while the dark blue highlights the low-density regions. During the cycle, by considering a 350 V battery and by using (7), the EM consumes a peak current of 270 A.

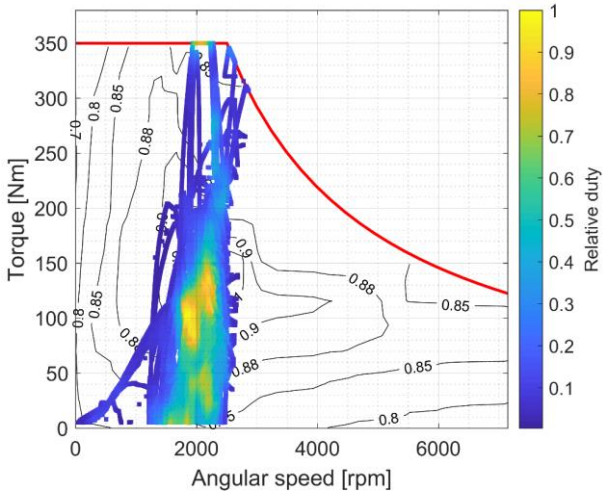


Figure 10. Plug-in torque working points during a WLTP cycle

### 5.1.2. Battery sizing

Once the EM is defined, the selection of the battery nominal capacity is conducted by aiming the best $CO_2$ emission reduction while minimizing the impact on the car in terms of added weight and dimensions. The $CO_2$ reduction and electric range are calculated according to the WLTP regulation.

Several simulations were run using a set of different battery sizes. For each simulation, the battery was initiated fully charged with a 95% SoC and one or several charge depleting (CD) cycles were run until the minimum SoC of 25% was reached. Subsequently, the CD cycles were followed by a single charge

sustaining (CS) cycle. Figure 11 shows the SoC variation during the various cycles. The first dashed red line at 3600 s marks the end of the n-1 CD cycles and the beginning of the transition cycle n. The second red dashed line at 5400 s marks the end of the transition cycle and the beginning of the CS cycle n+1. Additionally, the dashed black line at around 4800 s marks the $R_{CDA}$.

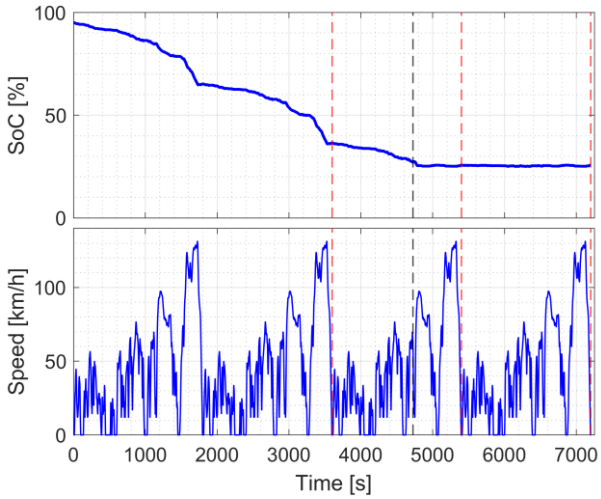


Figure 11. SoC and speed for a 30-kWh battery simulation.

Figure 12 shows the results obtained from the simulations at various battery capacities. For all the simulations, a battery pack specific energy of 113 Wh/kg [31] was used and the battery mass was adjusted when varying the capacity.

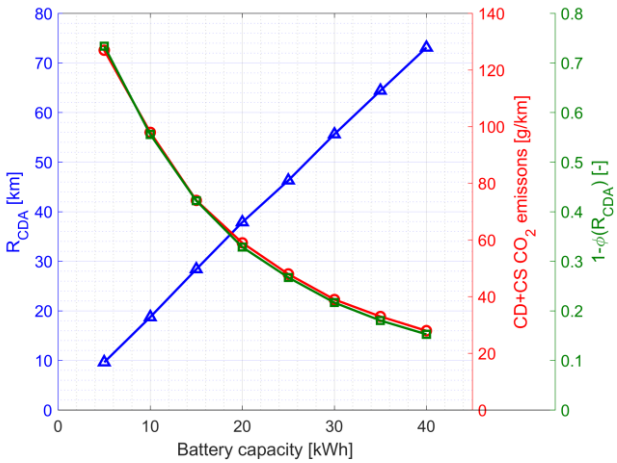


Figure 12. Simulation results: Actual charge depleting range, CO2 emissions and cumulative utility factor as a function of battery capacity.

The results (blue line) show that the range increases linearly with the battery capacity. This can be simply explained by the fact that both the electric energy stored in battery and the torque request, and therefore the requested energy during the test, increase linearly with the battery mass.

At any time instant, the force $F_{veh}$ requested by the vehicle can be expressed as:

$$F_{veh} = (M_{veh} + M_{batt})a + (M_{veh} + M_{batt})k_r g + F_{aer} \quad (11)$$

Where $M_{veh}$ is the vehicle mass excluding the battery, $M_{batt}$ is the battery mass, $a$ is the acceleration imposed by the cycle, $g$ is the gravitational constant, $k_r$ is the rolling resistance coefficient, and $F_{aer}$ is the aerodynamic drag which is independent of the battery mass.

The energy $E_{veh}$ requested to drive a certain distance is equal to

$$E_{cycle} = \int_{Range} F_{veh} v_{veh}\, dt \quad (12)$$

Where $v_{veh}$ is the vehicle speed imposed by the cycle, and $t$ is the time. Combining (4) and (5) it can be noted that the energy request increases linearly with the battery mass. Since the energy stored in the battery also increases linearly with $M_{batt}$, the range-battery size characteristic (blue line) is linear.

The two other curves (red and green line) instead show a strict correlation between the UF and the $CO_2$ emissions. Increasing the battery size from 5 to 20 kWh causes a drop of 68 g/km of $CO_2$, while increasing the battery capacity by the same amount from 20 to 35 kWh causes a decrease of only 26 g/km, indicating that there's a saturation in the $CO_2$ savings that is strictly correlated with the saturation of the UF. Therefore, the battery is sized at 25 kWh. Table 4 shows the results obtained from the simulations. The procedure used to calculate the average fuel consumption $FC_{CD+CS}$ is identical to the procedure used to calculate the average $M_{CO2,CD+CS}$.

Table 4. Simulation results at various battery capacities

| Description | Symbol | Unit | Values | | | | | | | |
|---|---|---|---|---|---|---|---|---|---|---|
| Battery pack capacity | – | kWh | 5 | 10 | 15 | 20 | 25 | 30 | 35 | 40 |
| Battery pack mass | – | kg | 44 | 89 | 133 | 177 | 221 | 266 | 310 | 354 |
| CS fuel consumption | $FC_{CS}$ | l/100 km | 6.52 | 6.57 | 6.64 | 6.69 | 6.74 | 6.79 | 6.83 | 6.90 |
| CD+CS fuel consumption | $FC_{CD+CS}$ | l/100 km | 4.74 | 3.68 | 2.76 | 2.19 | 1.80 | 1.46 | 1.24 | 1.05 |
| CD+CS CO2 emission | $M_{CO2,CD+CS}$ | g/km | 127 | 98 | 74 | 59 | 48 | 39 | 33 | 28 |
| CD actual charge depleting range | $R_{CDA}$ | km | 9.63 | 18.74 | 28.39 | 37.87 | 46.31 | 55.62 | 64.41 | 73.11 |
| Cumulative utility factor | $\phi(R_{CDA})$ | – | 0.27 | 0.44 | 0.58 | 0.67 | 0.73 | 0.78 | 0.82 | 0.85 |

The resulting battery characteristics are summarized in Table 5. The cell characteristics were obtained from [32]. The total battery pack voltage of 350 V was selected to be high enough to decrease the current, while also low enough as to not increase the required electronics cost. This value was found to be in line with automotive industry choices [33]. By knowing the voltage and capacity of the single cell and of the complete battery pack, the required cells series-parallel configuration can be deduced. Particularly, the pack voltage is guaranteed by the number of cells in series, while the pack capacity can then be obtained

by stacking the rows of in-series cells in parallel. Finally, the pack energy density and mass has already been introduced and is reported again for completeness.

Table 5. High voltage battery characteristics.

| Parameter | Value | Unit |
|---|---|---|
| Cell typical capacity | 5 | Ah |
| Cell nominal voltage | 3.7 | V |
| Battery pack voltage | 350 | V |
| Battery pack capacity | 25 | kWh |
| Cells arrangement | 15p95s | – |
| Battery pack specific energy | 113 | Wh/kg |
| Battery pack mass | 221 | kg |

It is worthy to note that by changing the cells arrangement the battery pack equivalent electrical resistance changes. A more in-depth analysis could attempt to optimize the cells configuration to maximize the efficiency of the system. However, the pack resistance is quite low with a marginal impact on the system overall efficiency.

## 5.2. Power-based approach

The mild hybrid P2 on axis is sized using a power-based approach. The EM is sized by analyzing the braking energy distribution during the cycle as a function of requested power and angular velocity. The energy recovery potential reaches an asymptote after a certain power level that is therefore chosen as the EM maximum power. The battery is sized by selecting a battery capable of supplying the EM with the required maximum current.

### 5.2.1. Electric machine sizing

According to the WLTP regulation, an NOVC HEV cycle has to be charge sustaining to be considered valid, i.e. the SOC at the end of the cycle must be equal to the SOC at the start of the cycle. Thus, all the energy used by the vehicle originates from the consumed fuel. Therefore, in order to improve

fuel economy, the EM must recover as much energy as possible during braking, as well as improving the ICE working points by boosting and power splitting.

Figure 13 represents the braking power request distribution during a cycle as function of EM speed. The yellow zones represent high density regions, with the highest density zone corresponding to 1 on the scale, while the dark blue zones represent low density regions. The EM should be able to recover most of the points without oversizing the motor power.

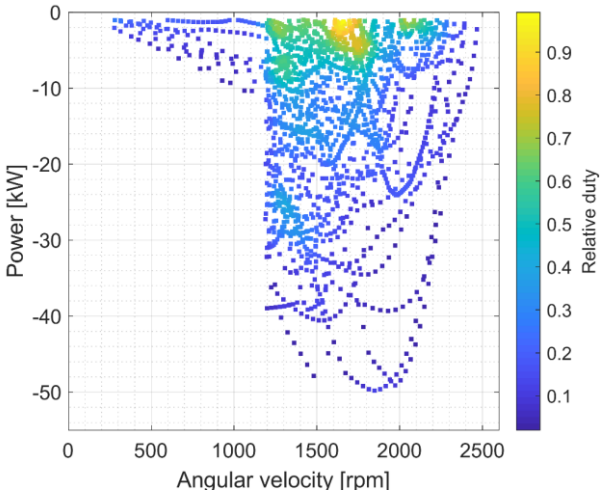


Figure 13. Requested braking power distribution as a function of EM angular speed during a WLTP cycle.

An EM power characteristic can be defined by the base speed $\omega_0$ and maximum power $P_0$. Once these two parameters have been fixed, the points of Figure 13 can be divided in two groups: the points that are covered by the EM characteristic and the points outside the power characteristic, as illustrated in Figure 14.

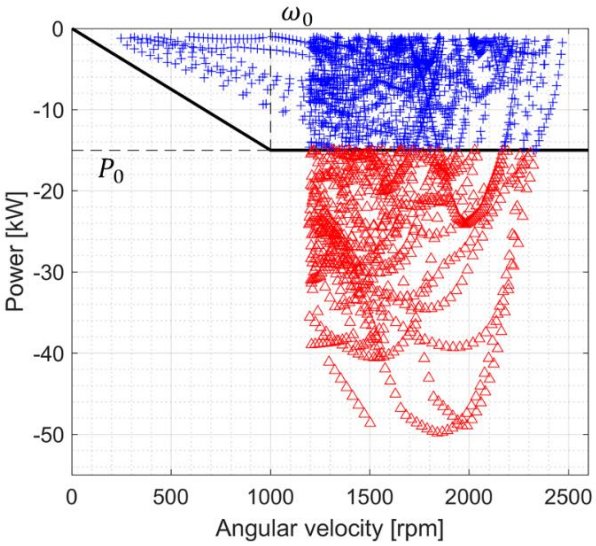


Figure 14. Requested power points divided by EM power characteristic. Blue cross: points inside the characteristic. Red triangles: points outside the characteristic.

The energy that can be recovered by a given EM is calculated considering that all the blue points inside the characteristic indicate energy that is recovered completely, whereas the red points outside the characteristic can only be partially recovered following the strategy that is graphically represented in Figure 15. For a point at speed $\omega$ the recovered power $P$ is equal to:

$$P_{rec} = \begin{cases} P_0 \dfrac{\omega}{\omega_0}, & \omega < \omega_0 \\ P_0, & \omega \geq \omega_0 \end{cases} \tag{13}$$

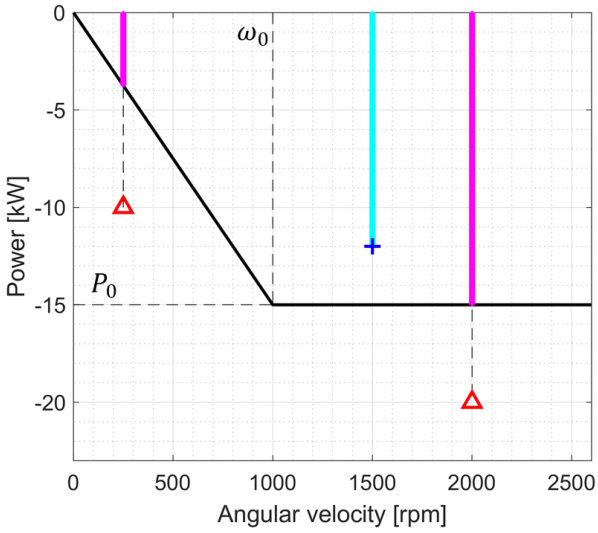


Figure 15. Power recovery by point as a function of EM power characteristic. Blue cross: point inside the characteristic: full recovery. Red triangle: point outside the characteristic: partial recovery. Teal and magenta lines: recovered power.

Lastly, by integrating the power recovered from all the request points over time, the recovered energy can be calculated. Figure 16 shows the percentage of recovered energy out of the total braking energy as a function of $P_0$ and $\omega_0$. For a given percentage, the chosen EM should have the lowest power. The volume and mass of the EM is proportional to the maximum torque of the EM, therefore for a given power and percentage the EM should have the highest base speed possible to reduce the mass.

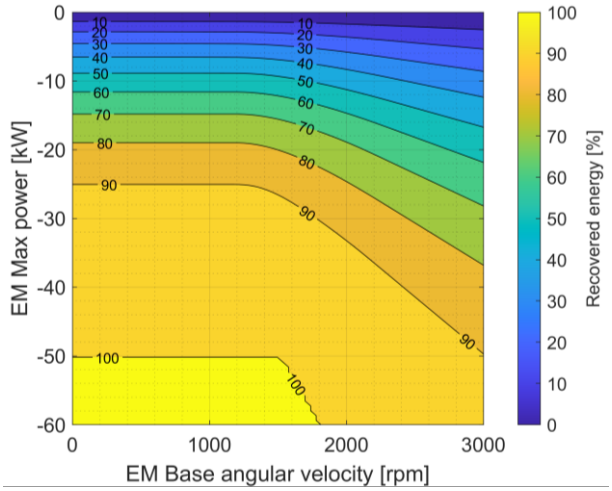


Figure 16. Recovered energy percentage as a function of EM maximum power and base speed.

From Figure 16, for a 90% recovery, the EM should have a maximum power of 24 kW and a base speed of 1500 rpm. By considering an EM with a symmetric power characteristic, i.e., with a motor characteristic that is equal and opposite to the generator characteristic, the characteristics of the EM are defined.

To validate the results, a series of simulations were performed using the EM whose torque characteristic is illustrated in Figure 17. EM features are also listed in Table 6. The EM max power $P_0$ was increased and decreased for each simulation while the base speed $\omega_0$ was maintained constant at 1500 rpm.

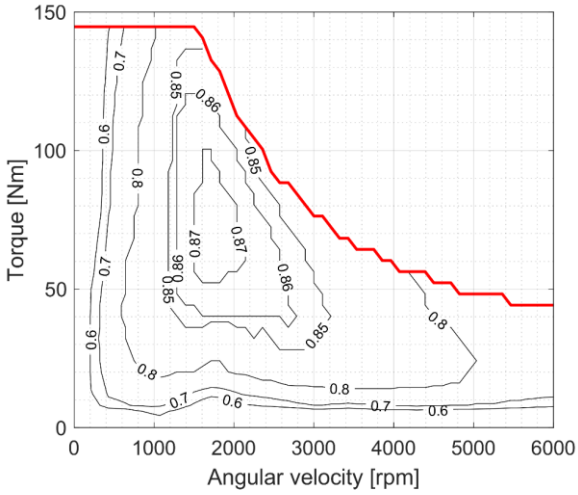


Figure 17. Low voltage EM torque characteristic and efficiency map.

Table 6. Low voltage EM features.

| Parameter | Value | Unit |
|---|---|---|
| Continuous torque | 55 | Nm |
| Peak torque (<10 s) | 147 | Nm |
| Base speed | 1500 | rpm |
| Max. speed | 6000 | rpm |
| Max. efficiency | 87 | % |
| PM flux linkage | 8.9 | mWb |
| Pole pairs | 14 | – |
| Phase-to-phase resistance | 3 | mΩ |
| Phase-to-phase inductance | 0.02 | mH |
| Saliency ratio | 0.41 | – |

The results presented in Figure 18 show a clear correlation between the fuel consumption and the recovered energy. As the recovered energy approaches 90% near 25 kW, the fuel savings reach an asymptote at around 17%.

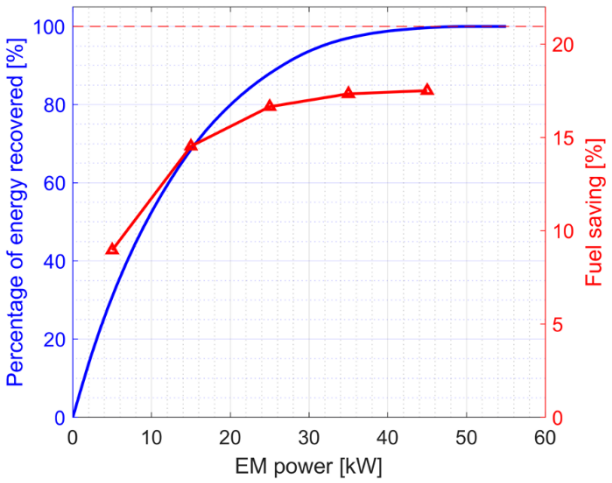


Figure 18. Recovered energy percentage (blue) and fuel savings percentage (red) for multiple EM power with a base speed of 1500 rpm.

### 5.02.2. Battery sizing

Using the battery model explained in Section 3.1, the power generated by the EM can be related to the power consumed in the battery following (14):

$$UI = P\eta + RI^2 \tag{14}$$

Where $P$ represents the EM power during generation (torque times angular speed), $\eta$ represents the efficiency and $U$, $I$ and $R$ represent the battery voltage, current and internal resistance, respectively. By solving (14), the current is calculated:

$$I = \frac{U - \sqrt{U^2 - 4R\frac{P}{\eta}}}{2R} \tag{15}$$

Considering an EM efficiency and maximum power of 0.8 and 24 kW respectively, corresponding to the EM base speed limit, and a battery voltage and internal resistance of 48 V and 10 mΩ respectively,

the maximum current during traction is equal to 739 A. Thus, considering a maximum battery discharge-rate of 15C [31], that can be sustained for a short time duration, the battery capacity is calculated at 49 Ah.

Similarly, the maximum current generated during braking can be calculated using (16):

$$I = \frac{U - \sqrt{U^2 - 4RP\eta}}{2R} \tag{16}$$

In this case, inserting the same values used to calculate the maximum traction current, the maximum braking current is equal to $-371$ A. Considering a lower charge rate of 10C, the necessary battery capacity is 37 Ah, which is lower than the capacity required for traction. Therefore, the battery capacity is sized at 49 Ah.

It is worthy to note that during a cycle, the battery SOC oscillations have a peak-to-peak amplitude of only $\sim 8\%$ as shown in Figure 19. This confirms that the battery capacity is more than enough to satisfy the energy storage needs.

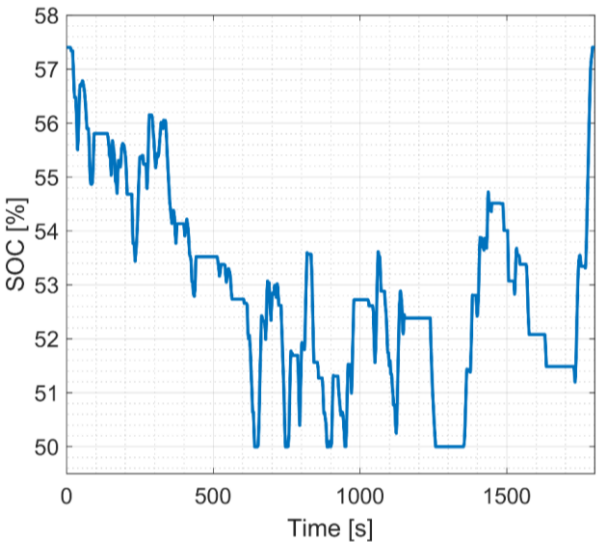


Figure 19. Battery SOC during WLTP cycle.

The resulting battery pack is shown in Table 7. The same battery cells used in Section 5.1.2 are again used to build the battery pack.

Table 7. Low voltage battery characteristics

| Parameter | Value | Unit |
|---|---|---|
| Cell typical capacity | 5 | Ah |
| Cell nominal voltage | 3.7 | V |
| Battery pack voltage | 48 | V |
| Battery pack capacity | 2.4 (49) | kWh (Ah) |
| Cells arrangement | 10p13s | – |
| Battery pack specific energy | 113 | Wh/kg |
| Battery pack mass | 21 | kg |

## 6. CONCLUSIONS

In this paper, an energy based unified battery and EM sizing method for OVC and NOVC vehicles was presented. This study considered a hybrid P2 vehicle architecture. A description of the vehicle model and its characteristics was provided along an illustration of the ECMS energy management strategy. The sizing for the OVC vehicle focused on the electric range and was therefore capacity based. The EM was sized with a peak torque of 350 Nm and a base speed of 2500 rpm, corresponding to a peak power of 92 kW, to allow all electric operation. The battery was selected with 350 V. It was demonstrated that the AER increases linearly with the battery size, while the $CO_2$ emissions reduction closely follow the UF trend. Thus, the possible reduction greatly diminished after a certain battery size. Therefore, the battery was sized at 25 kWh. The main advantage of this method is that it only requires a single simulation of the P2 vehicle on the WLTP cycle to perform a battery and EM sizing, allowing a quick and intuitive sizing. The sizing for the NOVC vehicle focused on energy recovery, and consequently relied on a power based method. The EM was sized by collecting all the required braking points during a WLTP cycle. The EM was then sized by choosing an EM capable of recovering 90% of all the available energy. Thus, a peak power of 24 kW

and a base speed of 1500 rpm were selected. The battery was sized at 49 Ah by limiting the maximum discharge rate at 15 C. Again, the main advantage of the method is that it allowed the sizing of the EM and battery using a single WLTP simulation, thus providing a quick solution.

Future work could aim at including the effects of the ICE downsizing in the method in case of the OVC vehicle. Additionally, in the case of a P2 vehicle the effects of the gear shifting schedule on the EM sizing could be implemented by further developing the energy management strategy and expanding the controller functions to the gear shifting.

## REFERENCES


[1] EU 2019/631. CO2 emission performance standards for new passenger cars and for new light commercial vehicles.

[2] EPA-HQ-OAR-2021-0208. Revised 2023 and Later Model Year Light-Duty Vehicle Greenhouse Gas Emissions Standards.

[3] GB 18352.6-2016. Limits and measurement methods for emissions from light-duty vehicles (CHINA6).

[4] Wei L. *Hybrid Electric Vehicle System Modeling and Control*. 2nd ed. John Wiley & Sons Ltd, 2017.

[5] Guzzella L and Sciarretta A. *Vehicle propulsion systems.* Vol. 1. Springer-Verlag Berlin Heidelberg. 2017.

[6] Emadi A. *Advanced Electric Drive Vehicles.* 1st ed. CRC Press, Taylor & Francis Group. 2015.

[7] McKay B. 48V architectures for enabling high efficiency (presentation). In: *Driving innovation workshop*, Continental AG, Washington, DC, 2016.

[8] Schaeffler. Mobility for tomorrow, Schaeffler Symposium 2018 https://www.schaeffler.com/remotemedien/media/_shared_media/08_media_library /01_publications/schaeffler_2/symposia_1/downloads_11/schaeffler_kolloquium_2018_en.pdf (2018, accessed 10 January 2022).

[9] Liao YG and Quail AM. Component sizing of traction motor in hybrid powertrains. In: *2011 IEEE Vehicle Power and Propulsion Conference*, Chicago, IL, USA, 2011, pp. 1–6.

[10] Sundström O, Guzzella L and Soltic P. Optimal Hybridization in Two Parallel Hybrid Electric Vehicles using Dynamic Programming. *IFAC Proceedings Volumes* 2008; 41: 4642–4647.

[11] Sundström O, Guzzella L and Soltic P. Torque-Assist Hybrid Electric Powertrain Sizing: From Optimal Control Towards a Sizing Law. *IEEE Trans Control Syst Technol* 2010; 18: 837–849.

[12] Lukic SM and Emadi A. Effects of drivetrain hybridization on fuel economy and dynamic performance of parallel hybrid electric vehicles. *IEEE Trans Veh Technol* 2004; 53: 385–389.

[13] Galdi V, Ippolito L, Piccolo A, et al. A genetic-based methodology for hybrid electric vehicles sizing. *Soft Comput* 2001; 5: 451–457.

[14] Castellazzi L, Ruzimov S, Bonfitto A, et al. A Method for Battery Sizing in Parallel P4 Mild Hybrid Electric Vehicles. *SAE Int. J. Elec. Veh* 2022; 11.

[15] Madanipour V, Montazeri-Gh M and Mahmoodi-k M. Multi-objective component sizing of plug-in hybrid electric vehicle for optimal energy management. *Clean Techn Environ Policy* 2016; 18: 1189–1202.

[16] Hou C, Wang H and Ouyang M. Battery Sizing for Plug-in Hybrid Electric Vehicles in Beijing: A TCO Model Based Analysis. *Energies* 2014; 7: 5374–5399.

[17] Wu X, Cao B, Li X, et al. Component sizing optimization of plug-in hybrid electric vehicles, *Appl Energy* 2011; 88: 799–804.

[18] Hu X, Moura SJ, Murgovski N, et al. Integrated Optimization of Battery Sizing, Charging, and Power Management in Plug-In Hybrid Electric Vehicles. *IEEE Trans Control Syst Technol* 2016; 24: 1036–1043.

[19] UN ECE/TRANS/180/Add.15/Amend.6. Technical Regulation on Worldwide harmonized Light vehicles Test Procedures (WLTP).

[20] Eder A, Schütze N, Rijnders A, et al. Development of a European Utility Factor Curve for OVC-HEVs for WLTP. Report, Appendix 1 – Utility Factors in: Riemersma I. Technical Report on the development of a Worldwide Harmonised Light duty vehicle Test Procedure (WLTP). https://www.unece.org/fileadmin/DAM/trans/doc/2015/wp29grpe/GRPE-72-02-Rev.1.pdf , January 2016.

[21] Plötz P, Funke SÁ. and Jochem P. Empirical Fuel Consumption and CO2 Emissions of Plug-In Hybrid Electric Vehicles. *J Ind Ecol* 2018; 22: 773-784.

[22] Plötz P and Jöhrens J. (2021): Realistic Test Cycle Utility Factors for Plug-in Hybrid Electric Vehicles in Europe. Report, Fraunhofer Institute for Systems and Innovation Research ISI, Karlsruhe , April 2021.

[23] MathWorks. Behavioral battery model, https://www.mathworks.com/help/physmod/sps/ref/battery.html (2008, accessed 20 January 2022).

[24] Mohan G, Assadian F and Longo S. Comparative analysis of forward-facing models vs backwardfacing models in powertrain component sizing. In: *IET Hybrid and Electric Vehicles Conference*, London, UK, 2013, London, 2013, pp.1–6.

[25] Puma-Benavides DS, Izquierdo-Reyes J, Galluzzi R, et al. Influence of the Final Ratio on the Consumption of an Electric Vehicle under Conditions of Standardized Driving Cycles. *Appl Sci* 2021; 11:11474.

[26] Onori S, Serrao L and Rizzoni G. *Hybrid Electric Vehicles: Energy Management Strategies.* 1st ed. Springer, 2016.

[27] Böhme TJ and Frank B. *Hybrid systems, optimal control and hybrid vehicles.* 1st ed. Cham, CH: Springer International, 2017.

[28] Hegde S, Bonfitto A, Rahmeh H, et al. Optimal Selection of Equivalence Factors for ECMS in Mild Hybrid Electric Vehicles. In: *Proceedings of the ASME 2021 International Design Engineering Technical Conferences and Computers and Informatio*n *in Engineering Conference. Volume 1: 23rd International Conference on Advanced Vehicle Technologies (AVT)*. Virtual, Online, 17 August–19 August 2021, paper no. DETC2021-71621, V001T01A019. ASME.

[29] Biswas A and Emadi A. Energy Management Systems for Electrified Powertrains: State-of-the-Art Review and Future Trends. *IEEE Trans Veh Technol* 2019; 68:6453-6467.

[30] Rahmeh H, Bonfitto A, Ruzimov S, et al. Fuzzy Logic vs Equivalent Consumption Minimization Strategy for Energy Management in P2 Hybrid Electric Vehicles. In: *Proceedings of the ASME 2020 International Design Engineering Technical Conferences and Computers and Information in Engineering Conference*. *Volume 4: 22nd International Conference on Advanced Vehicle Technologies (AVT)*. Virtual, Online, 17 August–19 August 2021, paper no. DETC2020-22431, V004T04A026. ASME.

[31] Marano V, Onori S, Guezennec Y, et al. Lithium-ion batteries life estimation for plug-in hybrid electric vehicles. In: *IEEE Vehicle Power and Propulsion Conference*, Dearborn, MI, USA, 2009, pp.536–543.

[32] Bonfitto A, Feraco S, Tonoli A, et al. Estimation accuracy and computational cost analysis of artificial neural networks for state of charge estimation in lithium batteries. *Batteries* 2019; 5(2):47.

[33] Car and Driver. Battery taxonomy: the differences between hybrid and EV batteries, https://www.caranddriver.com/news/a15345397/battery-taxonomy-the-differences-between-hybrid-and-ev-batteries ( 2021, accessed 12 April 2022)